Journal of System Design and Dynamics

Vol. 2, No. 1, 2008

Energy Transfer in a Three Body Momentum Exchange Impact Damper*

Lovely SON**, Hiroshi MATSUHISA** and Hideo UTSUNO**

**Department of Precision Engineering, Kyoto University,
Yoshida-honmachi, Sakyo-ku, Kyoto 606-8501, Japan
E-mail: lovelyson@std.mbox.media.kyoto-u.ac.jp

Abstract

Impact vibration such as a floor vibration caused by jumping of children or vibration of a press machine is very important engineering problem. The momentum exchange impact damper has been proposed to solve these problems. The basic principle of this damper is based on the energy transfer on collision of three body systems. However energy or momentum transfer at the impact is not explained theoretically. This paper considers the energy transfer incurred during collisions in three body systems. The three body systems considered herein consists of an impact mass, a main body and an absorber mass. When the impact mass collides with the main body, part of its kinetic energy is transferred to the main body. When the main body simultaneously collides with the absorber mass, part of the kinetic energy of the main body is transferred to the absorber mass. Consequently, the main body receives a small amount of shock and it is possible to keep the main body nearly stationary. In this study, the influence of contact frequency and natural frequency of the system on the energy transfer during collision is analyzed. A theoretical model is developed to analyze the effect of various system parameters. It is shown that the maximum transfer of energy that can be obtained occurs when the contact frequencies are the same. The theoretical analysis is validated with experimental results.

Key words: Impact, Vibration Control, Momentum Exchange, Absorber, Three Body Systems

1. Introduction

Impact vibration such as a floor vibration caused by jumping of children or vibration of a press machine is very important engineering problem. Adverse noise generation and large impact force transmission to the surrounding are the primary motivation for studying such problems. Many researchers have carried out studies in this area and a number of methods have been developed to solve such problems. In the early studies, the conventional tuned mass damper was used for control of impact induced vibration [(1)]. This method was shown to reduce the steady state response, but it fails to suppress the maximum peak of the transient response due to the delay of the damper motion. Application of active shock control with preview action was studied by Tanaka [(2,3)]. Even though this method could suppress the transient response, but it requires costly sensors and actuators to realize active control.

A method involving momentum exchange using an impact damper was proposed by Matsuhisa[(4,5)] to reduce the vibration and force transmission in impact vibration of floors and press machines. In the floor shock vibration control as reported in Matsuhisa[(4)], the impact damper is placed between the slab and the floor. The impact damper mass is contacted with the floor. When the floor receives an impact load, a part of kinetic energy of the floor is transferred to the absorber mass during collision. As the result, the floor vibration and the transmitted force to the slab decrease. In another application as reported in

*Received 16 Mar., 2007 (No. 07-0143)
[DOI: 10.1299/jsdd.2.425]

Matsuhisa[5], the impact damper is contacted to the press machine bed. The impact force received by this bed is partly transmitted to the impact damper during collision. Thus, the impact damper can reduce the bed vibration and the transmitted force to the ground. However, the effect of the contact condition between the main body such as floor and press machine and both the impact mass and the absorber mass has not yet been investigated.

In the case of collision between free rigid bodies, the energy transfer is influenced by the mass ratio and the coefficient of restitution. Generally the coefficient of restitution is used to introduce the energy losses during collision. However, in actual engineering application, the assumption of free rigid body collision is not valid, because the main body is elastic and it is supported by elastic structures.

Previously, researchers have conducted several studies focusing on the collision between free elastic balls. Herrmann and Seitz [6,7] conducted experimental and theoretical studies focusing on the modeling of collisions between several elastic balls. Reinsch[8] analyzed the perfect transmission of a linear chain of elastic balls. Ceanga and Hurmuzlu[9] developed an analytical method to predict the post impact velocities of several colliding elastic balls.

In this paper, two simple models, a spring-supported rigid rod and a free elastic rod, are used as the main body to study the energy exchange within an impact damper. The relationship between the natural frequency of the main body and the contact frequencies of the impact source and the impact damper are investigated theoretically and experimentally.

2. Rigid body collision

2.1 Solution by assumption of contact spring

The main body consists of a mass m supported by spring k. An impact source mass m_b collides m with initial velocity v_{b-}. Before collision, the impact damper mass m_d is contacting with m. When the collision takes place, as shown in Fig. 1, the momentum and the kinetic energy of m_b is transferred to m and m_d. The momentum and energy exchanges continue while the masses remain in contact with each other.

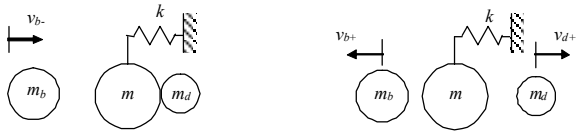

Fig. 1 Rigid body collision.

In this study, the contact condition is assumed to be given by linear springs k_b and k_d as shown in Fig. 2.

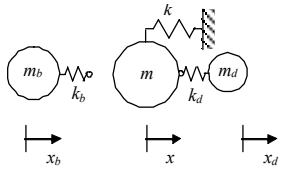

Fig. 2 Collision model of rigid body.

The governing equations of the three rigid bodies in Fig. 2 are given by

$$m_b\ddot{x}_b + f_b = 0\,, \tag{1}$$

$$m\ddot{x} + kx - f_b + f_d = 0\,, \tag{2}$$

$$m_d \ddot{x}_d - f_d = 0\,, \tag{3}$$

where x_b, x and x_d are the displacements of the impact mass, main body, and absorber mass, respectively. The variable f_b is the contact force between m and m_b and f_d is the contact force between m and m_d. These forces are given by

$$f_b = \begin{cases} k_b\left(x_b - x\right), & for \;\; x_b - x \geq 0, \\ 0, & for \;\; x_b - x < 0, \end{cases} \tag{4}$$

$$f_d = \begin{cases} k_d\left(x - x_d\right), & for \;\; x - x_d \geq 0, \\ 0, & for \;\; x - x_d < 0. \end{cases} \tag{5}$$

Integration of Eqs. (1)~(3) was carried out with MatLab/Simulink by using the fifth-order Dormand-Prince method with variable time steps. The transfers of energy from m_b to m_d and m after collision are calculated as

$$\frac{E_{d+}}{E_{b-}} = \frac{\frac{1}{2}m_d v_{d+}^2}{\frac{1}{2}m_b v_{b-}^2}, \tag{6}$$

$$\frac{E}{E_{b-}} = 1 - \frac{\frac{1}{2}m_b v_{b+}^2}{\frac{1}{2}m_b v_{b-}^2} - \frac{\frac{1}{2}m_d v_{d+}^2}{\frac{1}{2}m_b v_{b-}^2}, \tag{7}$$

where v_{b+} and v_{d+} are the velocity of m_b and m_d after collision.

When $f_b \neq 0$ and $f_d \neq 0$, the three masses remain in contact with each other. In this state the solution of Eqs. (1)~(3) is given by the combination of three harmonic functions relating to the natural frequencies of the system. The response of mass m_d is calculated as

$$x_d\left(t\right) = r_b \omega_b^2 \omega_d^2 v_{b-}\left[\frac{1}{\omega_1\left(\omega_1^2 - \omega_2^2\right)\left(\omega_1^2 - \omega_3^2\right)}\sin\omega_1 t - \frac{1}{\omega_2\left(\omega_1^2 - \omega_2^2\right)\left(\omega_2^2 - \omega_3^2\right)}\sin\omega_2 t\right.$$
$$\left. + \frac{1}{\omega_3\left(\omega_1^2 - \omega_3^2\right)\left(\omega_2^2 - \omega_3^2\right)}\sin\omega_3 t\right], \tag{8}$$

where

$$\omega_b = \sqrt{\frac{k_b}{m_b}}, \quad \omega_d = \sqrt{\frac{k_d}{m_d}}. \tag{9}$$

ω_1, ω_2 and ω_3 are the natural frequencies when the masses remain in contact. These natural frequencies are obtained by solving the characteristic equation of the system

$$s^6 + \left(\left(1 + r_b\right)\omega_b^2 + \omega^2 + \left(1 + r_d\right)\omega_d^2\right)s^4 + \left(\omega_b^2\omega^2 + \left(1 + r_b + r_d\right)\omega_b^2\omega_d^2 + \omega^2\omega_d^2\right)s^2$$
$$+ \omega_b^2\omega^2\omega_d^2 = 0\,, \tag{10}$$

where

$$r_b = \frac{m_b}{m}, \quad r_d = \frac{m_d}{m}, \omega = \sqrt{\frac{k}{m}}. \tag{11}$$

The velocity of m_d is obtained by differentiating Eq. (8)

$$v_d\left(t\right) = r_b \omega_b^2 \omega_d^2 v_{b-}\left[\frac{1}{\left(\omega_1^2 - \omega_2^2\right)\left(\omega_1^2 - \omega_3^2\right)}\cos\omega_1 t - \frac{1}{\left(\omega_1^2 - \omega_2^2\right)\left(\omega_2^2 - \omega_3^2\right)}\cos\omega_2 t\right.$$

$$+\frac{1}{\left(\omega_1^2-\omega_3^2\right)\left(\omega_2^2-\omega_3^2\right)}\cos\omega_3 t\Bigg]. \tag{12}$$

Suppose that m_b looses contact at $t = \pi/\omega_b$ and m_d looses contact after m_b, the velocity of m_d at $t = \pi/\omega_b$ is given by

$$v_d\left(\frac{\pi}{\omega_b}\right)=r_b\omega_b^2\omega_d^2 v_{b-}\left[\frac{1}{\left(\omega_1^2-\omega_2^2\right)\left(\omega_1^2-\omega_3^2\right)}\cos\frac{\pi\omega_1}{\omega_b}-\frac{1}{\left(\omega_1^2-\omega_2^2\right)\left(\omega_2^2-\omega_3^2\right)}\cos\frac{\pi\omega_2}{\omega_b}\right]$$

$$+\frac{1}{\left(\omega_1^2-\omega_3^2\right)\left(\omega_2^2-\omega_3^2\right)}\cos\frac{\pi\omega_3}{\omega_b}\Bigg]. \tag{13}$$

The maximum value of the first term in Eq. (13) is found when

$$\cos\frac{\pi\omega_1}{\omega_b}=1, \tag{14}$$

$$\frac{\omega_1}{\omega_b}=0,2,4,\cdots. \tag{15}$$

The maximum value of the second term in Eq. (13) is given by

$$\cos\frac{\pi\omega_2}{\omega_b}=-1, \tag{16}$$

$$\frac{\omega_2}{\omega_b}=1,3,5,\cdots. \tag{17}$$

The maximum value of the third term in Eq. (13) is obtained when

$$\cos\frac{\pi\omega_3}{\omega_b}=1, \tag{18}$$

$$\frac{\omega_3}{\omega_b}=0,2,4,\cdots. \tag{19}$$

Eqs. (15), (17) and (19) indicate that the maximum kinetic energy of m_d can be achieved when the ratio of the natural frequencies to ω_b are integer numbers.

In ideal case, ω_b should be as larger as possible to transfer a large amount of kinetic energy from m_b to m_d. Regarding this condition, the optimum value for the first term in Eq. (13) is achieved when

$$\frac{\omega_1}{\omega_b}=0, \quad \rightarrow \omega_1=0. \tag{20}$$

Substitution of $\omega_1 = 0$ into Eq. (10), indicates that the zero value of the characteristic root is obtained when

$$\omega_b^2\omega^2\omega_d^2=0, \ \rightarrow \omega=0. \tag{21}$$

For ratios of $\omega_r/\omega_b = 1$, ($r = 1,2,3,\cdots$), an optimum condition is obtained by substitution of $s^2=-\omega_b^2$ into Eq. (10), which yields,

$$\omega_b=\omega_d. \tag{22}$$

Equation (22) indicates that the optimum condition for transferring the energy is obtained when the contact frequencies are the same. Table 1 shows the parameter values

used in the simulation. One value of mass ratio m_b/m and four values of mass ratio m_d/m were used in the simulation. The natural frequency of mass m is fixed at 200π rad/s.

Table 1 Simulation parameters for rigid body collision.

Parameter	Value
m_b/m	0.5
m	1.8 kg
m_d/m	0.25, 0.5, 1, 1.5
ω	200π rad/s
v_{b-}	1 m/s

Simulation results for the energy transfer with mass ratios m_d/m = 0.25, 0.5, 1 and 1.5 are depicted in Fig. 3. The solid line is the transfer of energy (E_{d+}/E_{b-}) and the dashed line is the energy absorbed by the main body m (E/E_{b-}). It can be shown that the transfer of energy increases with increasing values of ω_b/ω. The peak transfer of energy and the point of minimum energy absorption are located close to point $\omega_b = \omega_d$ as indicated by Eq. (22). The mass ratio m_d/m is the significant factor in determining energy transfer. The minimum energy of main body is obtained when m_d/m =1. In this condition, wherein ω_b/ω=100, almost all of the kinetic energy of main body is transferred to the absorber mass as shown in Fig. 3(c).

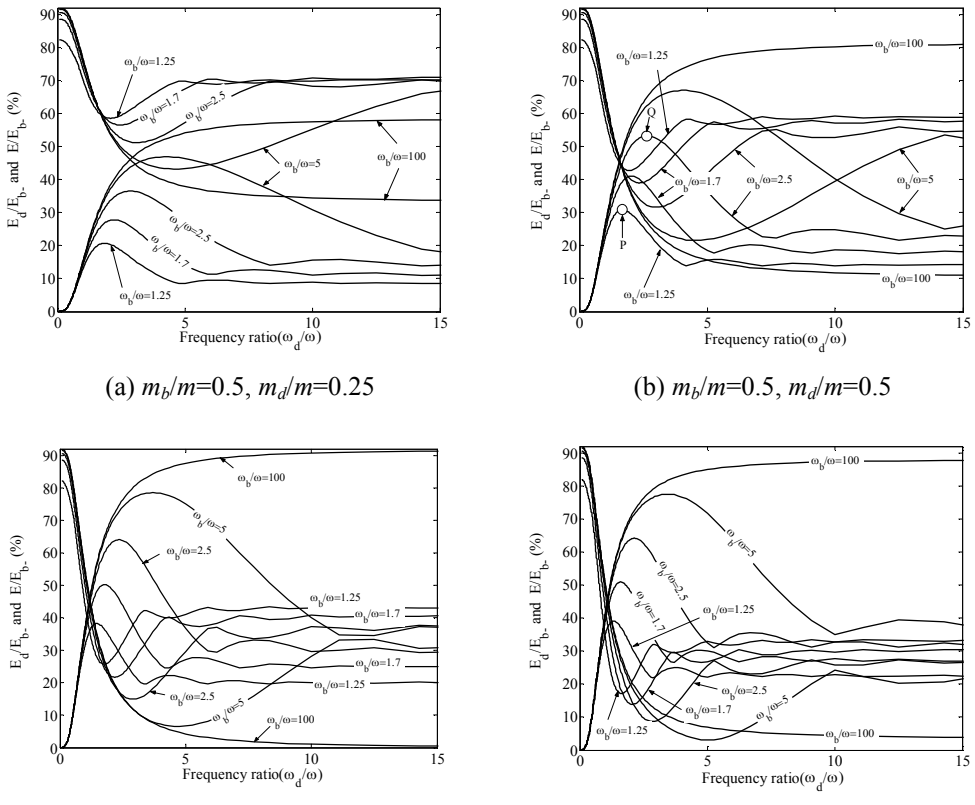

(a) m_b/m=0.5, m_d/m=0.25

(b) m_b/m=0.5, m_d/m=0.5

(c) m_b/m=0.5, m_d/m=1

(d) m_b/m=0.5, m_d/m=1.5

Fig. 3 Transfer of energy in collision of rigid bodies.
(solid line: E_{d+}/E_{b-}, dashed line : E/E_{b-})

Figure 4 and 5 show two sets of typical time responses of the system for ω_b/ω=1.25 and ω_b/ω= 2.5. These responses are obtained for mass ratios m_b/m = 0.5 and m_d/m 0.5. In these figures, force variables f_b, f_d and f_k were normalized by dividing them by $m_b\omega_b v_{b-}$. The velocity and time variables were also normalized by dividing them by v_{b-} and $\pi(m_b/k_b)^{1/2}$, respectively. As one might observe from these figures, the contact force f_b follows a nearly sinusoidal path for half a period after the impact. Figure 4 and Fig. 5 show that the velocity of m_d has a maximum value when ω_d/ω is located at the peak ratio of E_{d+}/E_{b-} (denoted by point P and Q in Fig. 3(b)). When ω_d/ω= 0.1, the velocity of m_d is small compared to the initial velocity of m_b. The reason for this is that the contact force f_d is small so that the transfer of momentum from m to m_d is low. The contact force f_d follows an un-smooth path for ω_d/ω=15. This phenomenon may be caused by multiple collisions. The multiple collision at ω_d/ω=15 occurs because the higher order mode of three bodies system are excited when mass m collide with mass m_d.

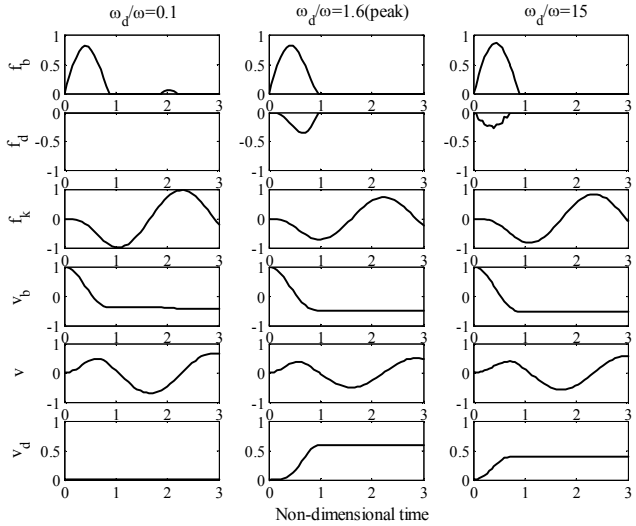

Fig. 4 Time history for ω_b/ω=1.25.

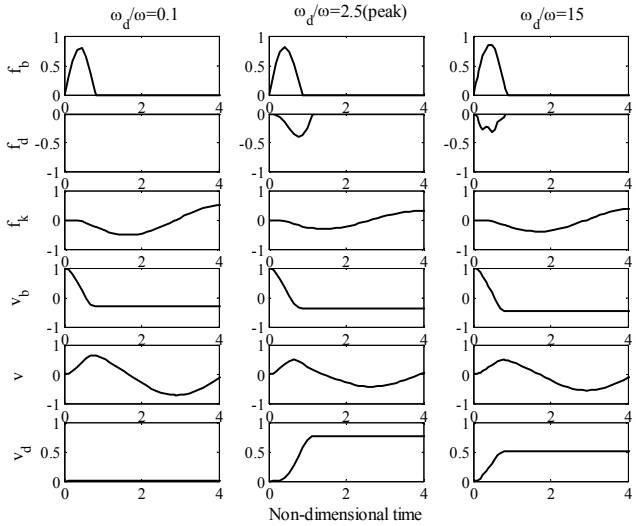

Fig. 5 Time history for ω_b/ω=2.5.

2.2 Solution using the coefficient of restitution

When $\omega_b >> \omega$ and $\omega_d >> \omega$, more energy is stored within the contact spring than in the oscillator spring [10]. This state can be regarded as a free collision problem. For this special case, the conservation of momentum and coefficient of restitution can be applied to the

collision between mass m and both m_b and m_d.

By using the conservation of momentum and coefficient of restitution for the first collision between m_b and m, yields

$$m_b v_{b+} + m v_+ = m_b v_{b-} + m v_- , \tag{23}$$

$$e_b = \frac{(v_+ - v_{b+})}{(v_{b-} - v_-)}, \tag{24}$$

$$J_b = (m v_+ - m v_-), \tag{25}$$

where v_- is velocity of m before the first collision, v_+ is velocity of m after the first collision, e_b is coefficient of restitution and J_b is impulse between m and m_b. Eqs. (23)~(25) can be arranged to give

$$J_b = \frac{m_b m}{m_b + m}(1 + e_b)(v_{b-} - v_-). \tag{26}$$

By using the same procedure for the second collision between m and m_d the following is obtained,

$$m v_{++} + m_d v_{d+} = m v_+ + m_d v_{d-}, \tag{27}$$

$$e_d = \frac{(v_{d+} - v_{++})}{(v_+ - v_{d-})}, \tag{28}$$

$$J_d = (m_d v_{d+} - m_d v_{d-}), \tag{29}$$

$$J_d = \frac{m m_d}{m + m_d}(1 + e_d)(v_+ - v_{d-}), \tag{30}$$

where v_{++} is velocity of m after the second collision, v_{d-} is velocity of m_d before the second collision, e_d is coefficient of restitution and J_d is impulse between m and m_d, respectively. In this case,

$$v_- = v_{d-} = 0. \tag{31}$$

By using Eqs. (23)~(24) and Eqs. (27)~(28), the final velocities of m_b and m_d are given by

$$v_{b+} = \frac{m_b - m e_b}{m_b + m} v_{b-}, \tag{32}$$

$$v_{d+} = \frac{(1 + e_b)(1 + e_d) m m_b}{(m + m_d)(m_b + m)} v_{b-}. \tag{33}$$

If $e_b = e_d = 1$, the final energy of mass m_b, m_d and m can be expressed as

$$\left(\frac{E_{b+}}{E_{b-}}\right)_{free} = \frac{\frac{1}{2} m_b v_{b+}^{\ 2}}{\frac{1}{2} m_b v_{b-}^2} = \left(\frac{m_b - m}{m_b + m}\right)^2, \tag{34}$$

$$\left(\frac{E_{d+}}{E_{b-}}\right)_{free} = \frac{\frac{1}{2} m_d v_{d+}^{\ 2}}{\frac{1}{2} m_b v_{b-}^2} = \frac{16 m^2 m_b m_d}{(m + m_d)^2 (m_b + m)^2}, \tag{35}$$

$$\left(\frac{E}{E_{b-}}\right)_{free} = 1 - \left(\frac{E_{b+}}{E_{b-}}\right)_{free} - \left(\frac{E_{d+}}{E_{b-}}\right)_{free}. \tag{36}$$

Equation (34) shows that the reflected energy is a function of m_b and m only. Increasing the mass ratio m_d/m only affects the final energy of mass m and m_d. When the mass ratio m_d/m =1, the final energy of m becomes zero.

Table 2 shows the results of final energy, calculated using Eqs. (34) ~ (36) for m_b/m = 0.5 and m_d/m = 0.25, 0.5, 1 and 1.5. The results in Table 2 agree well with the calculated results based on the contact spring model using Eqs. (1)~(5), as shown in Fig. 3 for $\omega_b/\omega \geq 100$.

Table 2 Final energy given by the coefficient of restitution method.

m_d/m	$\frac{E}{E_{b-}}$	$\frac{E_{b+}}{E_{b-}}$	$\frac{E_{d+}}{E_{b-}}$
0.25	0.33	0.11	0.56
0.5	0.1	0.11	0.79
1	0	0.11	0.89
1.5	0.03	0.11	0.85

3. Elastic rod collision

Figure 6 shows the model of a free one-dimensional elastic rod in collision with an impact source mass m_b. Mass m_d is initially in contact with the rod with zero initial velocity.

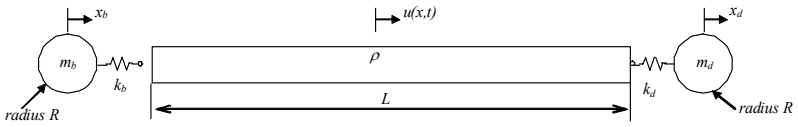

Fig. 6 Collision of free elastic rod.

The governing equations of motion are expressed as

$$\rho A\frac{\partial^2 u}{\partial t^2} - EA\frac{\partial^2 u}{\partial x^2} = 0;\ EA\frac{\partial u(0,t)}{\partial x} = f_b\ ;\ EA\frac{\partial u(L,t)}{\partial x} = -f_d, \tag{37}$$

$$m_b\ddot{x}_b + f_b = 0, \tag{38}$$

$$m_d\ddot{x}_d - f_d = 0, \tag{39}$$

where E is Young modulus, A is the cross section area and f_b and f_d are the contact force between rod and both m_b and m_d, respectively. The contact forces are given by

$$f_b = \begin{cases} k_b\left[x_b - u(0,t)\right], & for\quad x_b - u(0,t) \geq 0, \\ 0, & for\quad x_b - u(0,t) < 0, \end{cases} \tag{40}$$

$$f_d = \begin{cases} k_d\left[u(L,t) - x_d\right], & for\quad u(L,t) - x_d \geq 0, \\ 0, & for\quad u(L,t) - x_d < 0. \end{cases} \tag{41}$$

Longitudinal vibration of the rod can be given by summation of the normalized eigenfunctions $\psi_r(x)$ as

$$u(x,t)=\sum_{r=0}^{\infty}\psi_r(x)q_r(t), \tag{42}$$

where

$$\psi_r=\cos\frac{r\pi x}{L},\quad r=0,\cdots,\infty, \tag{43}$$

and q_r is the general coordinate. ψ_0 represents the non-vibrational rigid body transverse motion. By substituting Eq. (42) for u and using the orthogonality of the eigenfunctions, the differential equation of motion Eq. (37) can be written as [11]

$$\ddot{q}_r+\omega_r^2 q_r=\frac{f_r(t)}{m}, \tag{44}$$

where $f_r(t)$ is given by

$$f_r(t)=\int_0^L\left[f_b\delta(x-0)-f_d\delta(x-L)\right]\psi_r(x)dx, \tag{45}$$

and where $m=\rho A$ is the mass per unit length, $\omega_r=r\pi c/L$ is the natural frequency and c is the speed of sound for the rod and δ is delta function.

Two simulations using a steel rod with differing lengths were conducted to simulate the collision of rigid masses with an elastic rod. The simulation parameters were shown in Table 3, where $\omega_0\sim\omega_3$ are the natural frequencies of the rod.

Table 3 Simulation parameters of elastic rod collision.

Parameter	L = 2m	L = 3m
m_b	1 kg	1 kg
mL	5 kg	7.5 kg
m_d	1 kg	1 kg
A	7.85×10^{-5}m^2	7.85×10^{-5}m^2
v_{b-}	1m/s	1m/s
ω_0	0 rad/s	0 rad/s
ω_1	7.92×10^3 rad/s	5.28×10^3 rad/s
ω_2	1.58×10^4 rad/s	1.06×10^4 rad/s
ω_3	2.38×10^4 rad/s	1.58×10^4 rad/s

Numerical simulation was carried in MatLab/Simulink computational environment by using the fifth-order Dormand-Prince method with variable time steps. Variables ω_b and ω_d were varied within the range $\omega_b\in[6.6\times10^3,4\times10^4]$ rad/s and $\omega_d\in[1.6\times10^3,1.6\times10^5]$ rad/s.

Because the elastic rod is modeled as a continuous component, the system has an infinite number of vibration modes. Each mode contributes to the transfer of energy during the collision. Regarding to this condition, the simulation is conducted using 50 lowest modes of the rod.

Figure 7 shows the energy ratio (*EK*+*EP*) of the rod during collision. Before transferring the energy to m_d, the energy component of the rigid body mode (Energy mode 1) and the lowest elastic mode (Energy mode 2) are 37 % and 43% of the initial energy of m_b . After collision, the amount of energy transferred to m_d by the rigid body and the lowest elastic mode are 32.1 % and 39.5%, respectively. These results indicate that the contribution of the rigid mode and the lowest elastic mode to the transfer of energy is about 71.6% of the total energy. The contributions of other modes to the response are small compare to the rigid body and the lowest elastic mode contribution. Figure 7 shows that contribution of the 3rd

mode to the transfer of energy is about 13% and the contribution of the 4th, 5th and 6th mode are less than 5%. Regarding to this condition, only the first elastic mode is used for the discussion in this section.

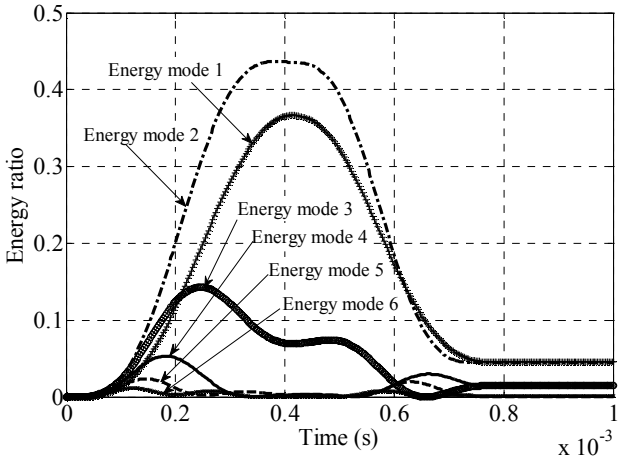

Fig. 7 Energy ratio of the rod during collision.

Figure 8 shows the simulation result of energy ratios as a function of ω_b/ω_1 and ω_d/ω_1 for rod lengths of 2 and 3 m. The solid line represents the transfer of energy (E_{d+}/E_{b-}) and the dashed line the energy absorbed by main body m (E/E_{b-}). Similarly to the previous case, the peak energy transfer and minimum absorbed energy are located near the point $\omega_b = \omega_d$. The transfer of energy is increases as ω_b/ω_1 is increased. For $\omega_d/\omega_1 > 5$ the transfer of energy is nearly constant.

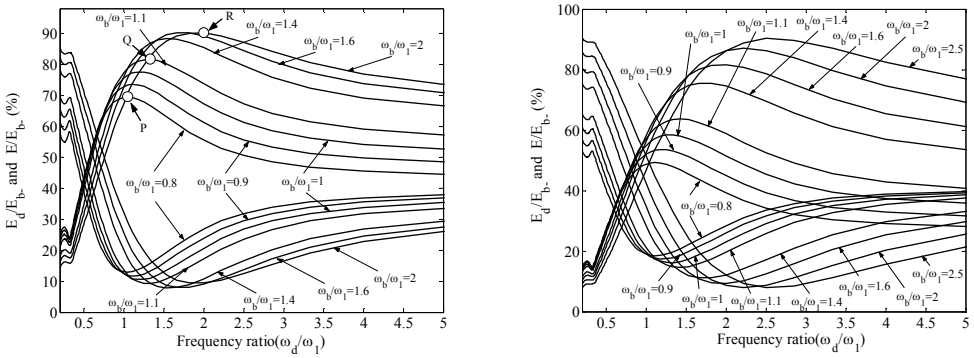

(a) L=2m (a) L=3m

Fig. 8 Transfer of energy of the free rod.
(solid line: E_{d+}/E_{b-}, dashed line : E/E_{b-})

It should be pointed out that the transfer of energy in the free elastic rod problem is partly governed by the elastic modes of the rod. This phenomenon is different from the transfer of energy in the free rigid body case described previously. For example, when the rod is assumed to be rigid, the transfer of energy calculated using Eq. (34) for a 2 m rod, yields

$$\frac{E_{d+}}{E_{b-}} = \frac{16m^2 m_b m_d}{\left(m+m_d\right)^2\left(m_b+m\right)^2} = 31\% . \tag{46}$$

This result is clearly lower than the resultant energy transfer shown in Fig. 8 (a) for the elastic rod. This is because its one-dimensional vibration modes were ignored in the

calculation.

Figures 9, 10 and 11 show three sets of typical time responses of the system for ω_b/ω_1 = 0.8, 1.1 and 2. These responses were obtained for L = 2m. In these figures, all variables were normalized according to the previously described criteria. Figure 9 shows that the velocity of m_d has a maximum value when ω_d/ω is located at the peak of the E_{d+}/E_{b-} curves (denoted by point P in Fig. 8(a)). The contact force f_d has two peaks for ω_d/ω_1 = 0.2 because the contact stiffness is small and the contact force is not large enough to make m_d loose contact simultaneously.

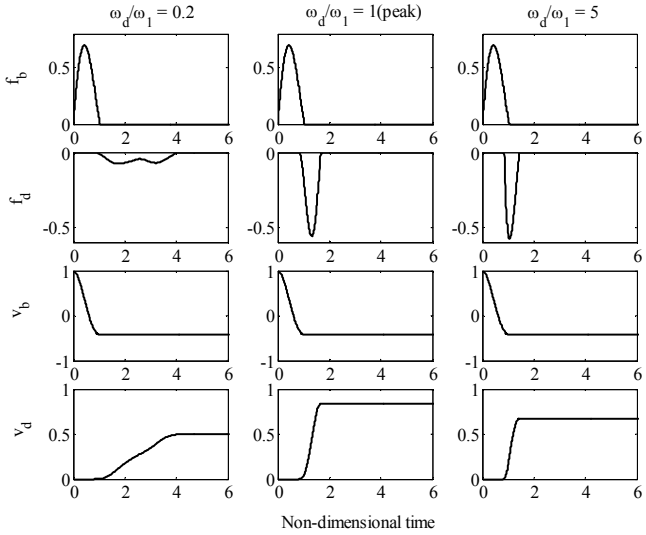

Fig. 9 Time history for ω_b/ω_1=0.8.

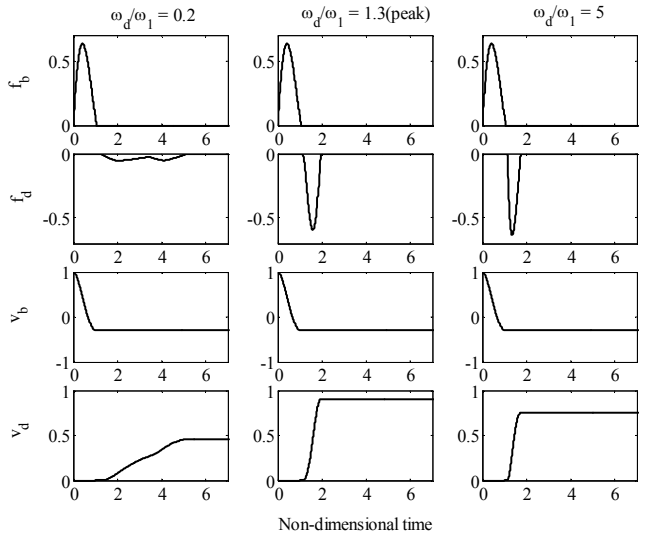

Fig. 10 Time history for ω_b/ω_1=1.1.

For small values of ω_b/ω_1 as shown in Fig. 9, the reflected velocity is almost 42% of the initial velocity of m_b (indicated by final velocity of m_b). In contrast, for large values of of ω_b/ω_1, as shown in Fig. 11, the reflected velocity is only 7%. In this case, nearly all of the kinetic energy of m_b is transferred to the rod.

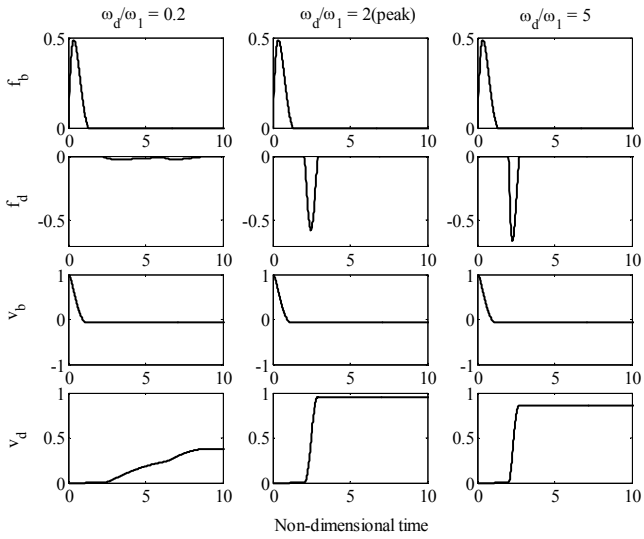

Fig. 11 Time history for ω_b/ω_1=2.

Figure 12 shows the displacement response of some lowest modes at the end of the rod where contacting with m_d. The displacement response from the 1st mode (the rigid body mode) has no time lag. The displacement response of the 2nd mode (the first elastic mode) occurs at different direction with the rigid body displacement. The responses from other modes are smaller in comparing to the 1st and the 2nd mode response. The total response of the rod (shown in the continuous line) is superposition of these modes response. As shown in Fig. 12, the total response has a time lag 0.4 ms. Regarding to this result, it can be concluded that the response of the rigid body mode has no time lag. The time lag obtained in the total response is due to superposition of the responses from each vibration modes.

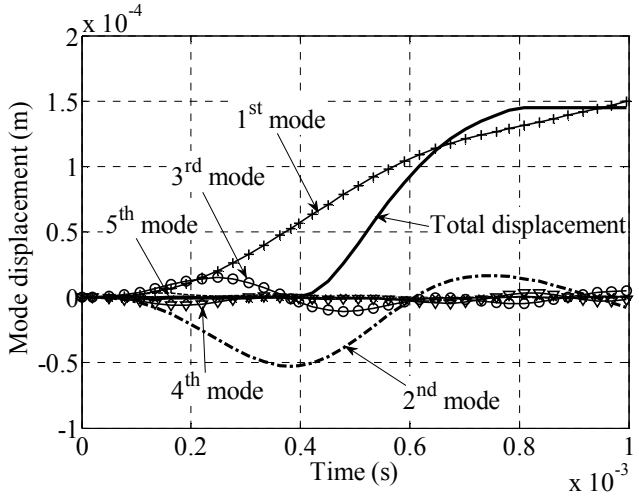

Fig. 12 Displacement response of some lowest modes at the end of the rod.

4. Experiment

In this chapter, two kinds of experiments the rigid body collision and elastic rod collision are carried out. In the experiment of rigid body collision problem on chapter 4.1, the contact surfaces are made of the golf ball and a short rod (0.6m). By using this configuration, the contact frequency between the rod and the rigid masses are much lower than the natural frequency of the rod elastic mode. In this case the collision problem can be regarded as the rigid body collision problem. For the experiment of elastic body collision problem on chapter 4.2, the contact surfaces are made of the steel ball and a long rod (2m).

By using this configuration, the contact frequency between the rod and the rigid masses are close to the natural frequency of the rod elastic mode so that the collision can be regarded as the elastic body collision problem.

4.1 Rigid body collision

An experimental apparatus consisting of two steel rigid masses and one short rod was used to validate the mathematical simulations. A golf ball was attached to each end of the rigid masses. The rigid masses were hung from a support frame by an aluminum arm (see Fig. 13). The impacts were obtained by releasing the first mass from a predetermined height. Table 4 shows the experimental parameters defining the rod and rigid masses. With this configuration it is possible to assume that the elastic modes of vibration can be neglected during impacted because ω_b and ω_d are small compared with the natural frequencies of elastic vibration.

Table 4 Experimental parameters for rigid body collision.

Parameter	Value
m_b	0.9 kg
mL	1.8 kg
m_d	0.45, 0.9 kg
h_{b-}	0.15 m
k_b	1×10^6 N/m
k_d	1×10^6 N/m
ω_b	1×10^3 rad/s
ω_d	1×10^3, 1.5×10^3 rad/s

The rod was supported by leaf springs on two supporting points to avoid yawing motion. The natural frequency of the supported rod was varied by altering the spring length and thickness. Table 5 shows the natural frequencies of the supported rod.

Table 5 Natural frequency of the supported rod.

No	Length of leaf spring (mm)	Thickness of leaf spring (mm)	k (N/m)	ω (rad/s)
1	32.15	4	6.1×10^6	2835.3
2	53.35	4	2.2×10^6	1562.9
3	31.30	1	1.8×10^5	477.5
4	42.85	1	7.3×10^4	318.9
5	97.50	1	8.9×10^3	95.5

The maximum height of m_b before collision and the maximum heigh of m_d after collision are measured by using a high speed camera. The transfer of energy from m_b to m_d was calculated by comparing the maximum height of m_d after collision to the maximum height of m_b before collision.

$$\frac{E_{d+}}{E_{b-}}=\frac{h_{d\max}}{h_{b-}}. \tag{47}$$

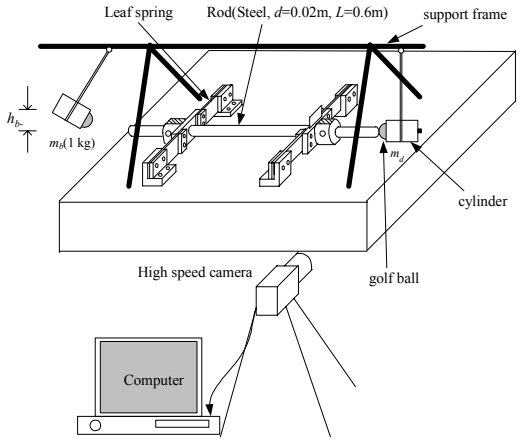

Fig. 13 Experimental apparatus for collision of rigid body.

Figure 14 shows the simulation and experimental result of the energy transfer, E_{d+}/E_{b-}. It should be pointed out that the results shown in Fig. 14 are for the special case, depicted in Fig. 3, wherein $k_b = k_d$. The transfer of energy that was obtained in the experimental was smaller than that calculated in the simulation. The difference is mainly due to energy losses from contact damping.

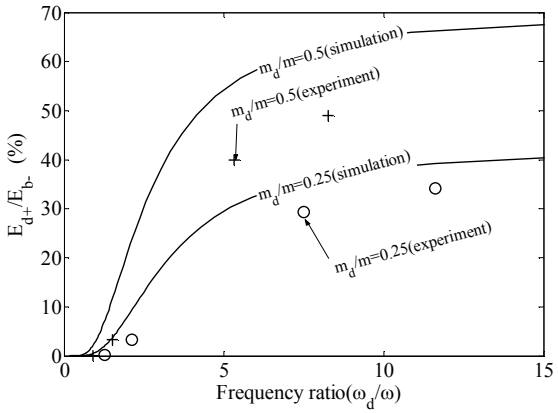

Fig. 14 Transfer of energy of rigid body.

Figure 15 shows the comparison of the acceleration time history of m_d obtained from the simulation and the experiment. T in Fig. 15 denotes the contact time obtained experimentally. As shown in Fig. 15, the acceleration at the end surface of the second cylinder resembled a single pulse and the amplitude of the subsequent periodic waves was reduced.

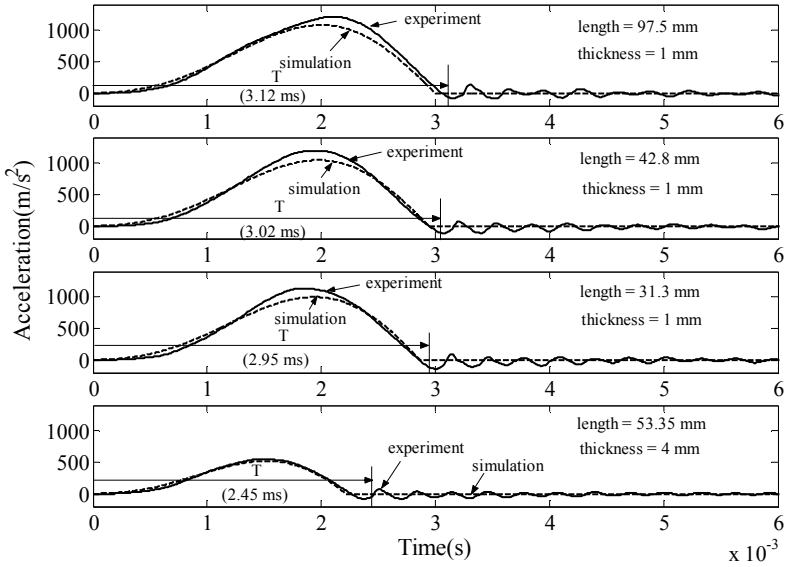

Fig. 15 Acceleration of m_d during collision.

4.2 Elastic rod collision

Figure 16 shows the experimental apparatus for the elastic rod problem. A long rod with a 2m length and 0.02 m diameter was hung using two wires. Two rigid masses m_b and m_d were positioned on each side of the rod. The initial height of m_b from its equilibrium position was 0.05 m, while m_d was initially contacting the rod. The rigid mode natural frequency of the rod is 6.2 rad/s. This frequency is small compared to the natural frequency of its first elastic mode and the contact frequencies ω_b and ω_d, which allows the rod to be assumed to be in a freely supported condition.

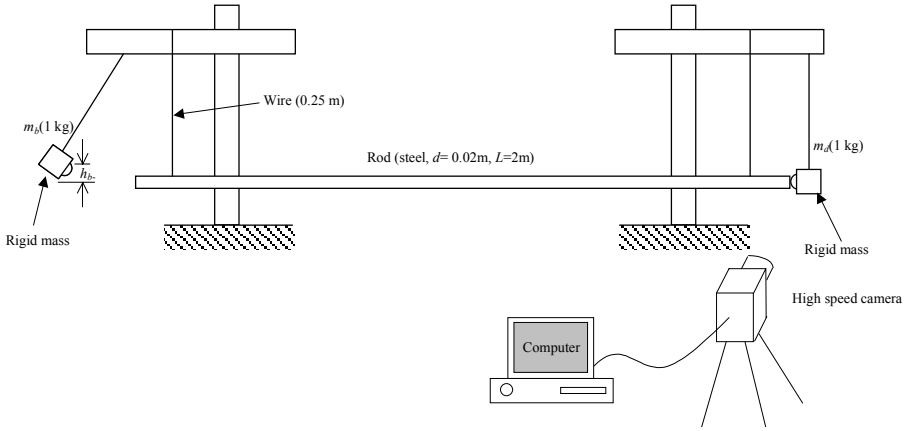

Fig. 16 Experimental setup for collision of elastic rod.

Variation of frequency ratio was obtained by using different contact stiffness. The contact stiffness between the rod and both m_b and m_d were determined by collisions with a rigid wall using the experiment set-up shown in Fig. 17. A mass is shown colliding with a rigid wall with initial velocity v_{b-}. The response of the mass during the collision was measured using an accelerometer. The contact duration was measured by using an electrical contact switch. The contact stiffness is obtained by reconciling the simulation results and the experimental data. Table 6 shows the calculated contact stiffness for four kinds of contact surfaces.

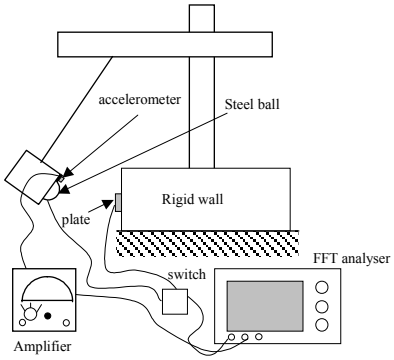

Fig. 17 Experimental setup for determining the contact stiffness.

Table 6 Contact stiffness and contact frequency.

Material of contact type	Contact stiffness (N/m)	Contact frequency(rad/s)
Steel ball(R=12.5mm)-steel plate	1.5×10^8	12000
Steel ball(R=12.5mm)-brass plate	8×10^7	8900
Steel ball(R=12.5mm)-aluminum plate	6×10^7	7700
Steel ball(R=12.5mm)-plastic plate	6×10^6	2400

The transfer of energy from m_b to m_d is shown in Fig. 18. Figure 18 shows that the simulation results and the experimental data are in good agreement. The differences in magnitude between simulation and experimental results are mainly due to contact damping.

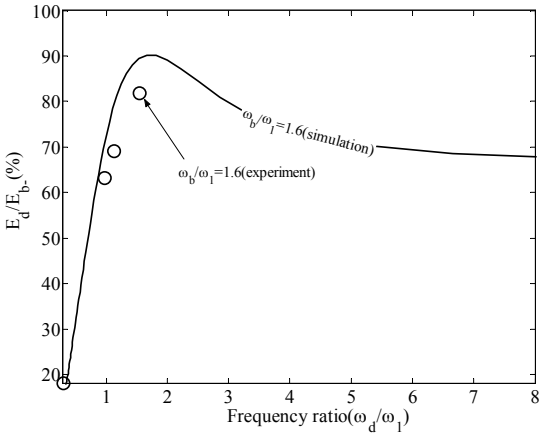

Fig. 18 Elastic rod energy transfer.

The difference between the experiment and the simulation result obtained from rigid body collision is larger than that obtained in elastic rod collision. For the rigid body collision, the rod is supported by the elastic spring. This supporting condition will introduce some energy loss due to friction damping. However, for the elastic rod collision, the rod is hanged by the wires so that the energy lose is very small.

5. Conclusions

The formulation and analysis of collision problems consisting of two rigid masses with a supported rigid rod and a free elastic rod has been presented. Although these are idealized systems, they can be used to simply model systems involving momentum exchange impact dampers.

For collision between rigid bodies, the maximum transfer of energy is obtained when

the natural frequency of the system in the contact state is the same as contact frequency between main body and both the impact mass (ω_b) and the absorber mass (ω_d). In this collision case, the mass ratio is significant in determining the transfer of energy. The amount of energy transfer increases as the contact frequency ω_b increases. When the frequency ratio between ω_b and natural frequency of main body greater than 100, the collision can be regarding as a free collision problem and the transfer of energy can be calculated using energy and momentum conservation.

For collision problems involving a free elastic rod, the maximum transfer of energy is obtained when the value of ω_b is close to that of ω_d. The transfer of energy is primarily governed by its elastic modes of vibration. In this case, changing the mass ratio does not significantly influence the energy transfer.

References

(1) Setareh, M., and Hanson, R.D., Tuned mass dampers to control floor vibrations from humans, *ASCE Journal of Structural Engineering*, Vol. 118(1992), pp.741-762.
(2) Tanaka, N., and Kikushima, Y., A Study on the dynamic damper with a preview action(1 st report, a principle of the dynamic damper with a preview action), *J. Jpn. Soc. Mech. Eng.*,(in Japanese), Vol. 52 No.484, C(1986), pp.3176-3183.
(3) Tanaka, N., and Kikushima, Y., A Study on the dynamic damper with a preview action(2 nd report, experiment of the dynamic damper with a preview action), *J. Jpn. Soc. Mech. Eng.*,(in Japanese), Vol. 53 No.487, C(1987), pp.650-655.
(4) Matsuhisa, H., Son, L., Reducing Floor Impact Vibration and Sound Using a momentum exchange impact damper, *Motion and Vibration Control Conference* (MOVIC), Daejeon, Korea(2006)
(5) Matsuhisa, H., Son, L., Application of momentum exchange impact damper on reducing the impact induce vibration on press machine, *The Third Asian Conference on Multibody Dynamics* (ACMD), Tokyo, Japan(2006)
(6) Herrmann, F., and Schmalzle, P., Simple explanation of well-known collision experiment, *Am.J.Phys.* Vol. 49(8)(1981), pp.761-764.
(7) Herrmann, F., and Seitz, M., How does the ball-chain work, *Am.J.Phys.* Vol. 50(11)(1984), pp.977-981.
(8) Reinsch, M., Dispersion-free linear chain. *Am.J.Phys.* Vol. 62(3)(1994), pp.271-278.
(9) Ceanga, V., and Hurmuzlu, Y., A New look at an old problem: Newtons Cradle, *Journal of Applied Mechanics*, Vol. 68(2001), pp. 575-583.
(10) Pinnington, R.J., Collision dynamics of two adjacent oscillators, *Journal of Sound and Vibration*, Vol. 268(2003), pp.343-360.
(11) Timoshenko, S., Vibration problems in engineering, *Jhon Wiley & Sons*, Fourth Edition(1974)